Engineering Cortical Neuron Polarity with Nanomagnets on a Chip

Anja Kunze,[*,†,‡] Peter Tseng,[†,‡] Chanya Godzich,[†] Coleman Murray,[†,‡] Anna Caputo,[§] Felix E. Schweizer,[§] and Dino Di Carlo[†,‡]

[†]Department of Bioengineering, [‡]California NanoSystems Institute, and [§]Department of Neurobiology, University of California, Los Angeles, California 90095, United States

ABSTRACT Intra- and extracellular signaling play critical roles in cell polarity, ultimately leading to the development of functional cell—cell connections, tissues, and organs. In the brain, pathologically oriented neurons are often the cause for disordered circuits, severely impacting motor function, perception, and memory. Aside from control through gene expression and signaling pathways, it is known that nervous system development can be manipulated by mechanical stimuli (*e.g.*, outgrowth of axons through externally applied forces). The inverse is true as well: intracellular molecular signals can be converted into forces to yield axonal outgrowth. The complete role played by mechanical signals in mediating single-cell polarity, however, remains currently unclear. Here we employ highly parallelized nanomagnets on a chip to exert local mechanical stimuli on cortical neurons, independently of the amount of superparamagnetic nanoparticles taken up by the cells. The chip-based approach was utilized to quantify the effect of nanoparticle-mediated forces on the intracellular cytoskeleton as visualized by the distribution of the microtubule-associated protein tau. While single cortical neurons prefer to assemble tau proteins following poly-L-lysine surface cues, an optimal force range of 4.5—70 pN by the nanomagnets initiated a tau distribution opposed to the pattern cue. In larger cell clusters (groups comprising six or more cells), nanoparticle-mediated forces induced tau repositioning in an observed range of 190—270 pN, and initiation of magnetic field-directed cell displacement was observed at forces above 300 pN. Our findings lay the groundwork for high-resolution mechanical encoding of neural networks *in vitro*, mechanically driven cell polarization in brain tissues, and neurotherapeutic approaches using functionalized superparamagnetic nanoparticles to potentially restore disordered neural circuits.

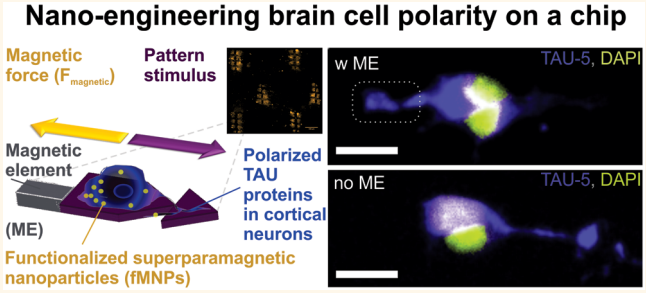

KEYWORDS: dissociated cortical neurons · protein polarization · tau · bipolar force interrogation · magnetic field gradients · magnetic BioMEMS · functionalized superparamagnetic nanoparticles

During brain development and neural network formation, a single neuron has to interpret multiple chemical[1,2] and mechanical signals[3−6] to functionally integrate with its neighbors to form a complex neural network. A crucial developmental step is cell polarization, which is defined in neurons through the asymmetric outgrowth of axons and dendrites from the soma.[7,8] During this step, the neuron has to organize its intracellular proteins toward opposing regions of the cell. Malfunctioning signal interpretation can trigger aberrant polarity of intracellular proteins, and cell polarization may occur in incorrect directions, resulting in neurological disorders.[9,10] An improved understanding of how neurons interpret disparate mechanical and chemical signals (ultimately resulting in protein polarization) is important for the development of neurotherapeutic approaches for such disorders or to improve whole brain neural cell models for computational approaches.[11]

Diverse *in vitro* platforms have widened our understanding of polarization in neurons, based on controlled and localized stimuli through biomolecule patterns, gradients, or geometrical boundaries.[12−14] Localized patterns of Sema3A cause undifferentiated neurites to become dendrites.[1] Axonal guidance has been achieved on surface patterns or through microfluidic-based gradients of poly-L-lysine (PLL) and laminin, where axons prefer to grow toward higher concentrations.[15−17] Geometrical shaping of neural cell adhesion molecules in the form of lines, gradient dots, and triangles locally guide neurites along PLL and laminin patterns[17−19] and support axonal growth preferentially toward the sharpest vertex in

* Address correspondence to akunze@ucla.edu.

Received for review September 19, 2014 and accepted March 23, 2015.

Published online March 23, 2015
10.1021/nn505330w

isosceles triangles.[18,20] In the developing brain, such molecular guidance cues compete with additional stimuli provided by, for example, (i) mechanical guidance by glial cells and connective tissue, (ii) metabolic or direct cell interactions (synaptic connections), and (iii) mechanical forces. In the latter case, Bok and Hilgetag pointed out a possible relationship between mechanical forces and differently shaped cortical neurons.[21,22] Tyler reviewed comprehensively how mechanical forces interfere with proteins that mediate neuronal signaling and plasticity in the brain.[23] However, the importance of biomechanical forces in mediating protein localization remains unclear. In particular, the magnitude of mechanical signals and their dependence on neighboring cellular and chemical stimuli remain unstudied. Research in the area of mechanical stimuli in neural networks has focused primarily on *in vitro* experiments with externally applied mechanical forces, on a variety of neurons and neuronal-like cell lines.[24−29] Using glass pipet tips or glass microfibers, neurites can be "pulled" from retinal ganglion cells, NG108-15, PC-12 cells, chicken forebrain neurons, and root dorsal ganglion, and axonal fate can be induced in hippocampal neurons.[25,27,30,31] Atomic force microscopy characterized force sensitivity of the soma[28] and of the axonal growth cone.[24] Accelerated axonal growth in response to stretching of an established dorsal root ganglion cell axon was demonstrated using a microstepper motor system.[26] Yet, these previous studies provide limited complexity compared to the brain environment, and the techniques employed are often low in throughput.

In biomechanics, cell-internalized functionalized superparamagnetic nanoparticles (fMNPs) are used within magnetic field gradients to study force-mediated intracellular signaling or to locally target signaling events within the cytoplasm.[32−34] The nanoparticle-mediated force approach has provided subcellular control of localized signaling pathways in non-neuronal cells, in dorsal ganglia,[33,35] and in retinal ganglions.[36] In contrast to previous studies, which focused on nanoparticle-mediated signaling events quantified by neurite outgrowth, orientation, or growth cone motility, we investigate here how nanoparticle-mediated forces impact the polarity of cortical neurons from the mammalian brain. Using nanomagnetic forces to engineer intracellular protein distribution, and even neuronal cell polarity, holds great promise, as these forces could potentially be generated directly in the brain, given that magnetic fields can easily penetrate brain tissues.[36]

To study locally well-controlled mechanical stimuli, current probing instruments such as magnetic tweezers are restricted to single-cell manipulation in series. The low-throughput factor was recently overcome through the development of a magnetic platform, which exposes thousands of arrayed cells to locally controllable stimuli induced through magnetic elements (MEs).[33] Due to the singular dimensions of the MEs, however, the nanoparticle-mediated force range could be controlled only through the amount of fMNPs taken up. Here, we designed a neuromagnetic chip that consists of multisized MEs on a glass chip able to attract cell-internalized nanomagnets (fMNPs, Figure 1). The multisized MEs allow us to tune the mechanical stimuli independent from the taken up amount of nanomagnets. Employing the neuromagnetic chip to dissociated cortical neurons, we studied the effect of distinct and localized nanoparticle-mediated force ranges on the intracellular distribution of microtubule-stabilizing proteins, tau, in single cells and cell clusters in a highly parallelized manner.

A previous study with internalized magnetic nanoparticles reported that neurite outgrowth can be put on hold in the low piconewton range,[36] suggesting that intracellular low piconewton stimuli might alter neuronal cell signaling transduction. Our study reveals that the localized mechanical stimuli affect the intracellular distribution of tau, before any change in neurite outgrowth can be measured. By fine-tuning the nanoparticle-mediated forces through engineered magnetic element sizes we observed an optimal force range for intracellular tau redistribution (in the lower piconewton range). In areas of larger cell populations, obtained by plating neurons on larger PLL striped patterns with increasing widths, neurons oriented their tau proteins randomly, likely due to competing cell neighbor interactions. Here, we found that a higher force magnitude was required to elicit directed tau polarity in growing neurons (two times higher). We observed that with increased mechanical stimuli, cells could be manipulated in the direction of the magnetic field gradients, potentially due to cell migration.

Finally, we demonstrate that our neuromagnetic chip is fully compatible with primary neuron incubation procedures and microscope setups, enabling further studies of force-directed synapse formation or calcium imaging studies. These chips can assist neuroscientists in better understanding the role of mechanical forces in neurons, and such strategies could potentially allow for the recapitulation of correct biological responses for cell and network models *in situ* and *in silico*.[11]

RESULTS AND DISCUSSION

For our study, we applied highly parallelized forces on chip to neurons in either single cell or cell population formation (Figure 1A,B). The single-cell area contains three repetitions of 48 arrays of 12 differently designed magnetic elements in combination with five different single-cell patterns, of which 5−8 arrays are exposed to an identical magnetic field flux (Figure 1B1 and Supporting Information Figure S2). Experiments in the single-cell area focused on bidirectional force perturbations,

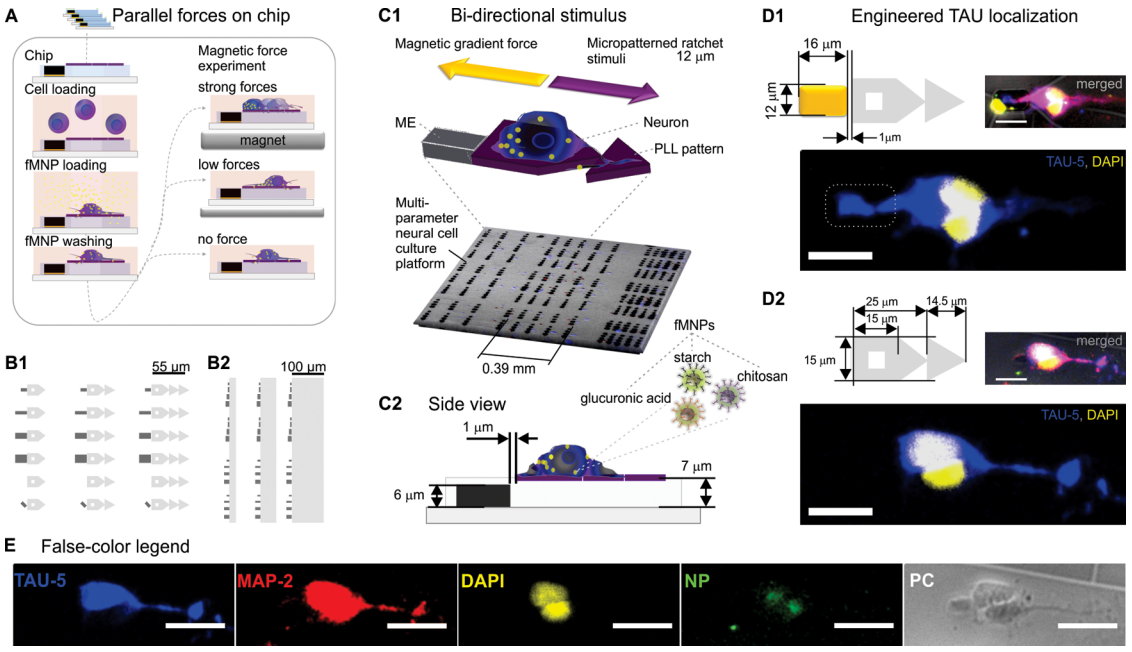

Figure 1. Engineering intracellular protein distribution on a multiparameter neuromagnetic chip. (A) Workflow to induce force stimuli by functionalized superparamagnetic nanoparticles (fMNPs) internalized within neurons, which leads to engineered tau protein polarity. (B1, B2) Cell adhesion (poly-L-lysine) and magnetic element (ME) patterns for highly parallelized (B1) single neuronal (arrowhead ratchets) and (B2) cell population (stripes) study. (B1) The arrowhead-shaped micropattern ratchets control neural cell positioning next to the MEs and stimulate directive tau localization in single neurons. Applying an opposed magnetic force adjacent to patterned single cells should provide easy access to quantify the cellular effect. (B2) Uniform PLL stripe patterns allow neurons to have a larger freedom to orient their cell bodies and intracellular proteins and to connect to cell neighbors, thus potentially representing a scenario more similar to the one a cell would encounter *in vivo*. (C1) Schematic showing a single cortical neuron positioned next to an ME. The micropatterned ratchet geometry biases tau protein formation away from the MEs before magnetic forces were applied. During magnetic force application the neuron gets exposed to a bidirectional stimulus. (C2) Neurons are shielded from ME materials through a planarizing layer of biocompatible photoresist. (D1, D2) Fluorescent images demonstrating engineered tau protein distribution in neurons on a geometrically shaped PLL pattern with (D1) and without (D2) opposed force stimulus. ME border is indicated by a dotted gray line. Scale = 16 μm. (E) False-color legend showing fMNP localization next to the cell nuclei, co-localized with intracellular markers such as MAP-2 and TAU-5. Scale = 20 μm.

where two opposing cues (nanoparticle-induced forces and adhesive pattern) acted in competition with each other on single neurons, for 24 h from day 1 to day 2 *in vitro* (DIV, Figure 1C). The cell stripe area maintains three repetitions of 27 arrays of five different stripe sizes, ranging from 20 to 150 μm, in combination with eight differently designed MEs, of which eight or nine arrays are exposed to an identical magnetic field flux at the same time (Figure 1B2). In the single-cell area, we evaluated over 600 single cortical neurons, and in the stripe area over 140 regions of interests (ROIs: 20 μm $\times$ 50 μm). For all experiments we used neurons dissociated from rat brain tissues (E18, cerebral cortex), which were subsequently cultured on our neuromagnetic chips. All cortical neurons were allowed to internalize fMNPs for 6 h before being exposed for 24 h to one of three different magnetic field strengths generated by a permanent magnet. The combination of (i) different field strengths, (ii) different magnetic element sizes and orientations, and (iii) different amounts and sizes of fMNP clusters yields a large combination of forces: from 4.3 pN to ~1 nN. Selected force ranges are shown for 100 and 150 mT external magnetic fields in Table 1. Force ranges for a 480 mT field were calculated assuming a linear scalable force strength acting on saturated fMNPs within magnetic field gradients. Thus, maximum force range can be assumed by applying 480 mT at large clusters of taken up fMNPs (category IV: ~200 pN $\times$ 4.8 = 960 pN, within its SD of ~1 nN). We studied the role of nanoparticle-mediated mechanical forces in biasing intracellular protein distribution, particularly by studying the asymmetric positioning of TAU-5 signaling (referred to as TAU) around the cell body using an orientation vector (Figure 1D1, D2 and Figure 3A, B). To visualize tau and other proteins, we used immunocytochemistry and wide-field as well as confocal microscopy. Only cells that were positive for specific neuronal cell markers, either TAU-5 or tubulin-3 (TUBULIN), were included in our evaluation (Figure 1 E).

Multisized Magnetic Elements Allow fMNP-Mediated Mechanical Stimuli Studies Independently of the Amount of fMNP Taken up. Primary cortical neurons take up fMNPs, with uptake speed, amount, and location differing based on the surface functional group. To understand mechanical stimuli effects that are independent of the amount of functional groups taken up (starch, chitosan, glucuronic acid), we designed a neuromagnetic chip with 12 multisized magnetic elements and exposed

TABLE 1. ME Size Dependent Force Ranges[a]

		logarithmic fit parameters for MP-induced forces				data set	extrapolated forces for NP clusters							
dimensions ME [size in μm × μm]	orientation [deg]	estimated F [pN]	SD [pN]	average decay [pN/μm]	SD [pN/μm]	nb [n.a.]	F [pN], SD [pN]							
		low external field, ⌀: 1 μm; pitch: 1 μm					group I		group II		group III		group IV	
12 × 16	length (0)	2.58	0.02	−0.026	0.002	3	14.1	0.1	26.0	0.2	92.5	0.8	113.1	1.0
12 × 16	rotation (45)	3.52	0.11	−0.028	0.001	4	19.3	0.6	35.4	1.1	126.3	3.9	154.4	4.7
12 × 16	vertical (90)	4.55	0.32	−0.039	0.002	3	25.0	1.8	45.9	3.3	163.5	11.6	199.8	14.2
12 × 16	rotation (45)	3.52	0.11	−0.028	0.001	4	19.3	0.6	35.4	1.1	126.3	3.9	154.4	4.7
8 × 16	rotation (45)	2.32	0.07	−0.026	0.002	3	12.7	0.4	23.4	0.7	83.5	2.6	102.0	3.1
4 × 16	rotation (45)	1.71	0.03	−0.018	0.001	3	9.4	0.2	17.2	0.3	61.4	1.1	75.1	1.4
4 × 8	rotation (45)	1.19		−0.023	0.001	1	6.6		12.0		42.9	0.0	52.4	0.0
		medium external field												
12 × 16	length (0)	3.88	0.03	−0.0118	0.0003	3	21.3	0.2	39.1	0.3	139.4	1.0	170.4	1.3
4 × 16	length (0)	1.58		−0.0021	0.0004	1	8.7		15.9		56.7		69.2	

[a] Legend: nb, number of data sets with individual data points >100; SD, standard deviation; NP, nanoparticles; MP, microparticles; ⌀, particle/cluster diameter; pitch, distance to magnetic element (ME). Different nanoparticle cluster sizes: group I, ⌀ = 0.8 μm, $A < 0.5\ \mu m^2$ (29.8%); group II, ⌀ = 0.98 μm, $A = 0.5-1.0\ \mu m^2$ (15.0%); group III, ⌀ = 1.5 μm, $A = 1.0-2.0\ \mu m^2$ (14.8%); group IV, ⌀ = 1.6 μm, $A > 2.0\ \mu m^2$ (32.6%).

neurons to a mixture of fMNPs with different functional groups (Figure 2; see Supporting Information Figures S5 and S6). Previous studies have reported neuronal uptake of glucuronic acid-coated iron oxide nanoparticles.[37,38] We used these particles, in combination with starch- and chitosan-coated fMNPs, to prevent biased cell response due to potential differences in pathway-specific uptake of the nanoparticles and specific interactions with fMNP surface charges.[39]

For our experiments, the optimal cell viability with fMNP uptake was obtained following a 6 h incubation period. A 6 h incubation time resulted in a large range of intracellular fMNPs, shown in Figure 2A−C, which we classified into different groups: group 0, neurons that contained no nanoparticles (7.8%); group I, neurons that contained few nanoparticles with $A_{cluster} < 0.5\ \mu m^2$ (29.8%); group II, neurons that showed few spots between $A_{cluster}$ 0.5 μm^2 and 1.0 μm^2 (15.0%); group III, neurons that had few or multiple spots of $A_{cluster}$ 1.0 μm^2 between 2.0 μm^2 (14.8%); and group IV, neurons that contained fMNP clusters with $A_{cluster} > 2.0\ \mu m^2$ (32.6%).

To study mechanical effects almost independent of the distribution and amount of functional groups taken up of intracellular fMNPs within a cell culture, we came up with the idea to alter the magnetic field gradient through multisized MEs (Figure 2D1). The local deformation of the magnetic field yields strong magnetic field gradients, which exert forces on fMNPs and locally trap them next to the MEs (eq 1).[33,38,40] Instead of applying one constant magnetic gradient, we modulated the size and orientation of the MEs to generate unique and multiple local magnetic field potential minima. Local magnetic forces scaled with (i) the size and orientation of the MEs, (ii) the distance from the MEs, (iii) the externally applied permanent magnetic field, and (iv) the amount and cluster size of nanoparticles (eq 2, Table 1).

We used 6 μm thick MEs of four varying sizes and three selected orientations, embedded within our chips, to study force stimuli in cortical neurons in a variety of piconewton ranges. The MEs were minimally 83 μm spaced apart. We observed that a magnetic field direction that was slightly offset in relation to the axis of the MEs attracted fMNPs to dominant edges of the ME, called trap points (see Supporting Information Figure S2). In the case where fMNPs are further away from the first-order trap point, they become trapped at a second- or third-order trap point. For the most dominant trap points, estimated forces for different fMNP clusters were calibrated in relation to ⌀ 1 μm ferromagnetic microparticles at a pitch of 1 μm away from the ME. Further, it was assumed that fMNP clusters assembled roughly into a spherical shape, which was confirmed by confocal microscopy (Figure 2B1−3, Supporting Information video V1, eqs 7 and 8). However, for other cell types, the cluster formation might show other assembly forms, *e.g.*, a disk shape form due to membrane confinement. In this case the force would scale down with a factor $(4/3)r_h h_c^{-1}$, where h_c is the confinement height and r_h the hydrodynamic radius of the particle cluster.

The combination of interacting nanoparticles and ME parameters yields an active force range from 4.3 pN to ~1 nN with an average percentage force error of 3%. A selection of obtained force ranges according to ME sizes, orientations, and different groups of fMNPs taken up are reported in Table 1. A cellular response, *e.g.*, in the range 4.3 to 15 pN, can be studied within group I and II neurons by selecting the corresponding smaller length and rotational-oriented MEs. The force range

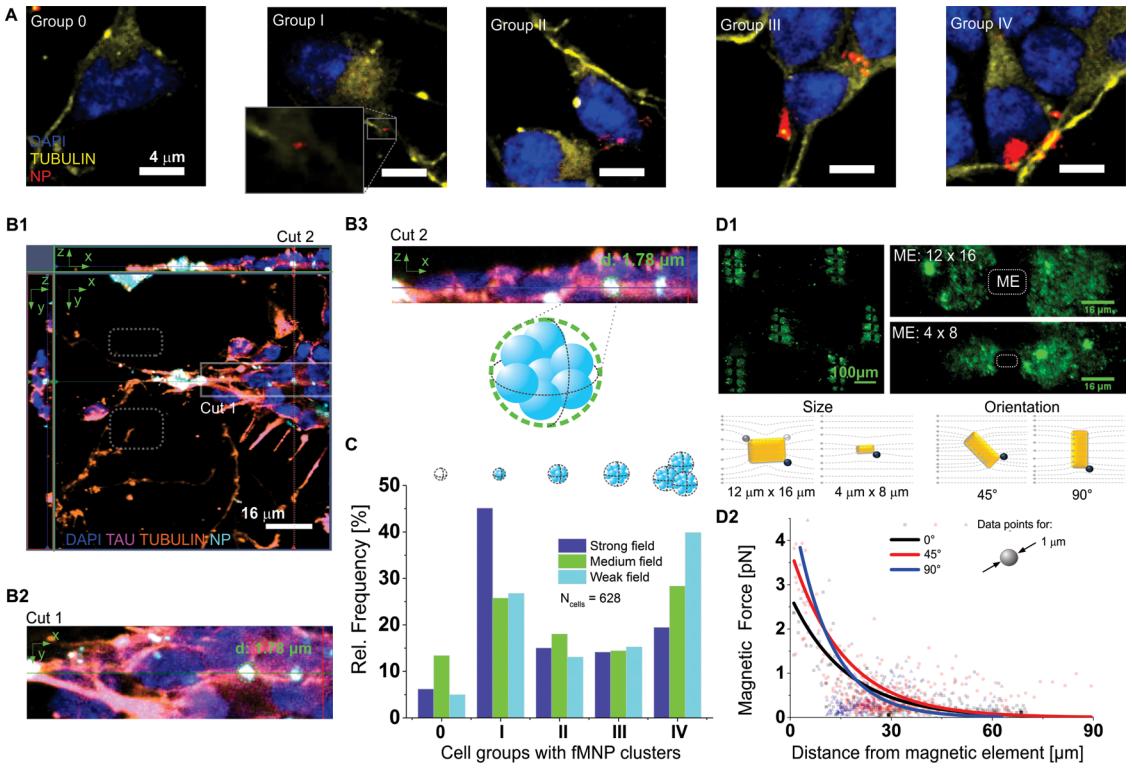

Figure 2. Multisized magnetic elements homogenize force stimuli of different amounts of fMNPs taken up in cortical neurons. (A) Multiple sized clusters of fMNPs induced different force ranges in neurons. Laser confocal images show example neurons assigned to five different classes of fMNP clusters after a 6 h incubation. Scale = 5 μm. (B1) Fluorescent confocal images of neurons after 24 h exposure to magnetic forces on chips highlight fMNPs co-localized with cytoskeleton proteins tubulin and TAU-5. (B2, B3) Subimages highlight spherical cluster appearance of fMNPs taken up and used to extract different force ranges. (C) Relative data distribution of cell groups within grouped clusters of fMNPs. (D1) Different ME sizes and orientations generate different magnetic field gradients to which fNMPs (green), here in suspension, get attracted and trapped. Local trap points are shown in first (dark gray = strongest), second (gray), and third (light gray = weakest) order. (D2) Magnetic force plot shows ME orientation-dependent force gradients and maximum force amplitudes for 12 μm $\times$ 16 μm MEs and three different orientations.

from 30 to 70 pN comprises all groups of neurons with fMNPs, resulting in a cellular effect that is independent of the amount of fMNPs taken up.

Nanoparticle-Mediated Forces Impact Tau Polarity in Single Neurons. On our neuromagnetic chip, cortical neurons were isolated from the underlying magnetic elements through a planarizing layer of biocompatible photoresist.[41] On top of the photoresist, local PLL cell adhesion patterns were photolithographically defined next to the magnetic elements. The highest cell adhesion was obtained when the biocompatible photoresist surface was plasma treated through a photoresist-defined stencil, and poly-L-lysine/pluronic (PLL/Pluronic) were coadsorbed following resist stripping.[42,43] The shapes of the PLL/Pluronic cell adhesion patterns are similar to those used by Scott *et al.* and Mahmud *et al.*,[20,44] who showed directed cell migration and neurite guidance along arrowhead geometries. This arrowhead geometry was used to design our micropatterned ratchets to direct tau protein orientation away from the MEs. Intracellular tau protein distribution was quantified through a phosphorylation-independent marker (TAU-5, Figure 3A). The costaining of TAU-5 with MAP-2 can be used to discriminate dendrites from axons (see Supporting Information Figure S7), but here we focused only on tau. In addition to the TAU-5 immunostaining, to determine whether the fMNPs can interact with the neuronal cytoskeleton, we visualized and found co-localization of fluorescent signals from fMNPs (white punctate spots) with neuronal markers of the cell cytoskeleton (tubulin-3, MAP-2 in Figure 2B).

Due to the early developmental stage of neurons in culture (stage 2, <3 DIV),[17,45] we pinpointed the centroid of the fluorescent intensity of TAU-5 and quantified its position in relation to the nucleus centroid as a reference point (Figure 3A). This derived orientation vector tends to correlate within 180° of the orientation of axonal outgrowth in stage 3 (5 DIV) neurons, yielding an approximation of eventual axonal polarity (in Supporting Information Figure S7). Quantifying protein distribution through this orientation vector allowed us to determine the spatial orientation of tau proteins within the cells by either projecting this vector length on the stimuli axis or examining the vector angle, and this is a general metric of single-cell polarity (Figure 3B).

Neurons cultured on large, uniform PLL patterns exhibited randomized orientation vectors, as we found

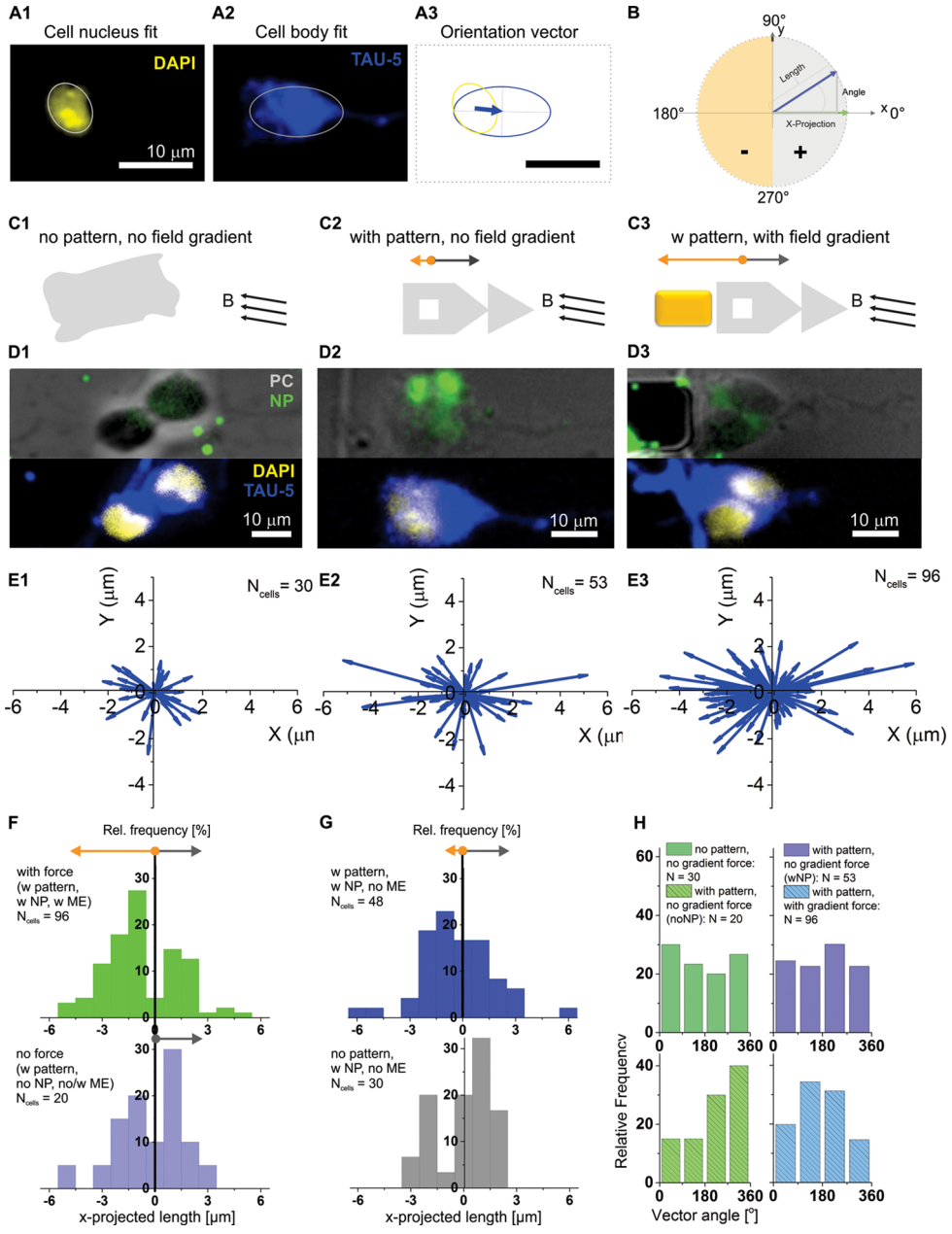

Figure 3. Polarized tau distribution follows magnetic gradient forces mediated by fMNPs under medium magnetic fields (150 mT). (A1−A3) Quantifying intracellular TAU-5 protein polarity based on the position of the nucleus centroid (A1, DAPI) and TAU-5 distribution with localized high signal intensity in somata (A2, TAU). (A3) Our orientation vector connects the two centroids pointing from elliptical fits and points toward the highest intracellular TAU-5 fluorescent intensity signal. (B) The orientation vector yields two plot parameters, its *x*-projected length and the orientation angle parallel to the pattern axis. (C1−C3) Three extracted parameter groups show the impact of the pattern and localized forces on TAU-5 distribution. All cells were loaded with fMNPs for 6 h and exposed for an additional 24 h to a medium magnetic field with indicated directionality (gray arrows). (D1−D3) Fluorescence images highlight representative 2-day-old neurons *in vitro* after 24 h exposure to medium magnetic fields for the above parameter group. (E1−E3) Parameter group corresponding to orientation vector plots, with significant shifts toward the magnetic field gradient ($p < 0.05$), when fMNP-induced force ($F > 6.5$ pN) was applied. (F) Relative frequency distribution plot of binned lengths of projected orientation vectors (13 bins) in a pattern with (w: with fMNP, with ME) and without forces (no fMNP, no ME). (G) Impact of pattern and small-scale, fMNP-induced, forces $F < 6.5$ pN. (H) Binned angle histogram for TAU-5 distribution in neurons cultured on a uniform PLL surface *versus* geometrically shaped PLL pattern and on a PLL pattern with and without opposed fMNP-induced forces.

the tau-derived orientation vector circularly distributed around the nuclei centroid (Figure 3C1, D1, and E1). When neurons were seeded on the PLL micropatterned ratchets and contained no fMNPs, 55% of the cells were oriented parallel to the micropatterned ratchet and generally preferred angle orientations between 270° and 360°, likely indicating that eventual neural outgrowth would be oriented in the direction of the ratchet (Figure 3F and H). These findings are similar to oriented neurite and axonal outgrowth reported for

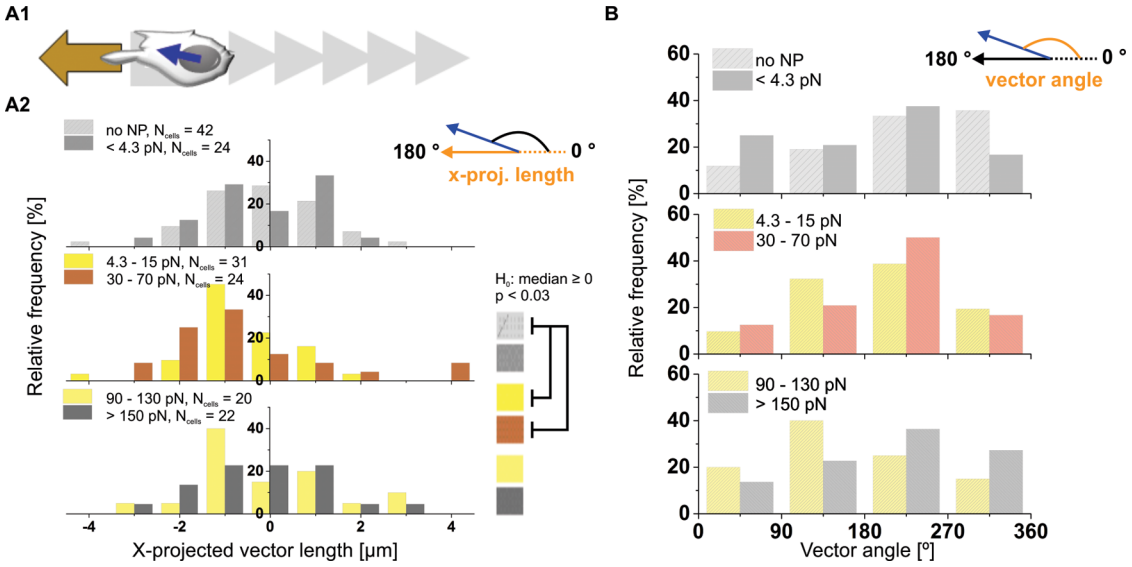

Figure 4. Parameter-grouped cell response based on binned force ranges revealed an optimal particle-mediated force range to drive tau protein relocation between 4.3 and 70 pN. (A1) Optimal force range to engineer intracellular protein polarity was assessed through orientation vectors pointing from nuclei to intracellular-located TAU-5. (A2) Frequency histogram of binned *x*-projected vector lengths shows optimal force range between 4.3 and 130 pN to relocate tau proteins. Statistical significance is present only in the 4.3−90 pN force range (nonparametric hypothesis test, $p < 0.05$, H_0 = no force effect, when median ≥ 0). (B) Binned angle histogram shows noncircular distribution of TAU-5 proteins when neurons were exposed to a magnetic field gradient (w ME, force range 4.3−130 pN).

hippocampal neurons after 48 h of growth on stripes of triangles[20] or other neuronal morphological constraints.[46] Interestingly, when neurons contained fMNPs (Figure 3E2, G), their vector orientation was slightly impacted, similar to findings by Riggio *et al.*[40] In our experiments, however, without ME forces, these results were not significantly different from a test median = 0. Comparing the histogram of cells next to MEs (under magnetic force influence) with cells under no force influence indicates a significant shift of tau distribution toward the MEs ($p = 0.02$: normality rejected, $p = 0.001$: median <0, Figure 3F and E3) and an increase of vector angles between 90° and 180° (Figure 3H). For all four conditions in Figure 3, medians of vector lengths were significantly different from each other ($p < 0.05$, Kruskal−Wallis ANOVA). In summary, exposing cortical neurons to ME induced force gradients above 6.5 pN for medium magnetic fields and relocated the position of tau distribution with orientation toward the force cue, thus impacting cell polarization in opposition to the micropatterned ratchets.

Engineered Neuronal Polarity within an Optimal Force Range of 4.3−70 pN. After observing indications of force-dependent protein polarity in single neurons, we examined if the polarization effect scales with increased forces. We increased the external magnetic field strength from 100 mT to 480 mT and grouped our results into six distinct force ranges based on combinations of ME sizes and fMNP clusters (Table 1). The distribution of the *x*-projected orientation vectors and also the orientation angle for the selected force ranges are shown in Figure 4. The histogram plots of the *x*-projected orientation vectors demonstrate a shift of the median toward the direction of our MEs for forces between 4.3 and 70 pN, with the longest vector lengths in the 30−70 pN force range. We tested the median of the histogram against an ideal test median = 0 (null-hypothesis) and found the force range 4.3−70 pN to induce a significant difference (Figure 4A, $p < 0.05$). Thus, the force threshold for tau polarity seems to be similar to reported force thresholds for neurite outgrowth values reported by Steketee *et al.*[36] and by Fass *et al.*[25] Now, in the force range 90−130 pN, the median of the orientation vectors was not significantly different from the test median = 0 ($p = 0.11$). In addition, when increasing the permanent magnetic field up to ∼450 mT, we estimated generating forces at the neural cell membrane up to ∼1 nN (Table 1: largest H-oriented ME, cluster bin IV, 480 mT external field). Our 2-day-old cortical neurons, however, did not show *x*-projected orientation vectors pointing toward the negative *x*-axis above 130 pN. There are three possible explanations for the reduced effect of tau polarization above 130 pN: (i) neurons change their cell behavior under higher forces, (ii) cortical neurons are incapable of responding to higher absolute forces or high force differences across the soma (∇F), or (iii) the induced high force ruptures the cell membrane, resulting in cell death similar to the reported detaching of force-modulated microbeads from the soma above 350 pN.[25] While our current data allow no final conclusion on the second case, we do have indications for the first case, that neurons change their cellular behavior under

higher force. Neurons that were exposed to strong magnetic fields were often located on the last arrow of the ratchet pattern, when MEs were lacking (see Supporting Information Figure S9). In contrast, we observed a higher amount of neurons close to MEs when they were present, potentially indicating that cells were physically manipulated to migrate toward magnetic field gradients, presumably accompanied by a change in cellular behavior. Furthermore, in Figure 4B vector angle plots show a shift of angle distribution from the 180−270° quadrant for 30−70 pN to the 90−180° quadrant for 90−130 pN, which can be interpreted as a sign of cellular reorganization due to cell displacement or changes in cellular behavior.

In regard to the third case and potential for cell death at high forces, we have analyzed only neurons that were still attached after washing and fixation. Interestingly, a relatively high number of these neurons contained a low amount of fMNP clusters taken up after exposure to strong magnetic fields, in contrast to the weak and medium magnetic fields (Figure 2C). This result is consistent with cell death and de-adhesion of cells from the substrate with higher levels of magnetic particles/forces. Further investigations elucidating the range of force responses are discussed below.

From our experimental data we infer that cortical neurons are particularly sensitive to moderate forces, in the range of 4.5 to 70 pN. Within this force range immunostaining of the intracellular protein tau showed increased fluorescent signal in the cell side adjacent to the ME. This observation was drawn from a variety of neurons exposed to the same force range with different levels of internalized fMNPs. Tau is a very soluble protein within the neuronal cytoplasm.[47,48] Above 130 pN we observed a drift in cell response, most likely corresponding to observed cell displacement. It seems unlikely, although not impossible, that tau directly interacts with the fMNPs. More plausibly, fMNPs push against the cytoskeleton, intracellular organelles, or the cell membrane, and these disruptions lead to a change in neuronal polarity visualized by tau. Dynamically visualizing many proteins and organelles will be necessary to gain more mechanistic insight into the chain of events.

Neurons with Neighbors Compete against Higher Network Strength and Can Be Displaced above 300 pN. In the cortical tissue, neurons are integrated in a dense neurite network, potentially impacting their sensitivity to nanoparticle-mediated forces. To quantify this cell population sensitivity, cortical neurons were cultured on uniform PLL stripes, where they can have potential cell−cell contact to defined cell neighbors due to the confined pattern width (Figure 5). The PLL pattern and molecular/physical interplay of nearby cells produce a competing stimulus, against our magnetic forces, similar to topographical changes shown by Gomez *et al.*[49] Our neuromagnetic platform, however, allows us to quantify the forces, in addition to showing the effect qualitatively. In our data set we compared neurons on stripe widths of 100, 50, and 20 μm with 12 $\pm$ 5 neighbors per cell (N_{data} = 49), 5 $\pm$ 1 neighbors per cell (N_{data} = 61), and 2 $\pm$ 1 neighbors per cell (N_{data} = 80; $p < 0.001$, one-way ANOVA, normally distributed). To facilitate data interpretation, we sectioned the stripes into three force zones of decreasing force each of 33 μm width (Figure 5A1, A2). Independently of the pattern width, neurons were exposed to forces of 18−304 pN, 8.7 pN/μm in zone 1 *versus* forces of 0.8−16.5 pN, 0.48 pN/μm in zone 2 or forces of 0.04−0.7 pN, 0.02pN/μm in zone 3 when situated next to 12 μm $\times$ 16 μm, 0° oriented ME with medium magnetic field exposure (150 mT, Figure 5B2). Without a magnetic force gradient, neurons in zones 1 and 3 outgrew their neurites onto the PLL stripes and followed pattern boundaries (Figure 5B1) similar to cell responses reported by Banker *et al.* and Shelly *et al.*[17,50] In contrast, neurons in zone 2 oriented neurites only toward cell neighbors (Figure 5B1, middle). With local magnetic gradients, neurons in zone 1 grew neurites in parallel toward the fMNP trap points (Figure 5B2). Neurons in zone 2 seemed to show a weaker orientation effect, and neurons in zone 3 possess a similar morphology to the null force condition (Figure 5B2). For statistical comparison, we performed normalized averages (n = 9−12) of the fluorescence intensity from cell nuclei (DAPI), fMNP (NP), and neuronal markers (MAP2, TAU-5, and Tubulin) (Figure 5C1, C2). Neural cell populations with 12 $\pm$ 5 neighbors per cell and exposed to moderate magnetic fields (without MEs) displayed a uniform cell assembly (DAPI, Figure 5C1) across the 100 μm PLL pattern with no significant differences between cell distribution in zone 1 *versus* zone 3 (nonparametric, Kruskal−Wallis ANOVA, p = 0.19). In contrast, DAPI signal increased in zone 1 when magnetic elements were present (Figure 5C2). Furthermore, under micromagnetic gradients, DAPI, MAP-2, and the NP intensity distributions were significantly shifted toward the magnetic gradient in comparison to no magnetic gradients (Friedman ANOVA, $p < 0.005$), but not the tau distribution, indicating that large magnetic fields can induce neurons to displace toward gradients. This cell displacement was also observed on smaller PLL patterns with 5 $\pm$ 1 neighbors per cell and showed an increased cell ratio (zone 2 *versus* zone 1; see Supporting Information Figure S10). In this case, however, tau distribution shifted significantly, too. We assume that the force range here was high enough to displace and polarize neurons with 5 $\pm$ 1 neighbors per cell but could only displace neurons with 12 $\pm$ 5 neighbors per cell, indicating that tau polarization is impacted by cell−cell forces (see Supporting Information Figure S10).

Evaluating different force ranges on the 5 $\pm$ 1 neighbors per cell case yielded a force threshold

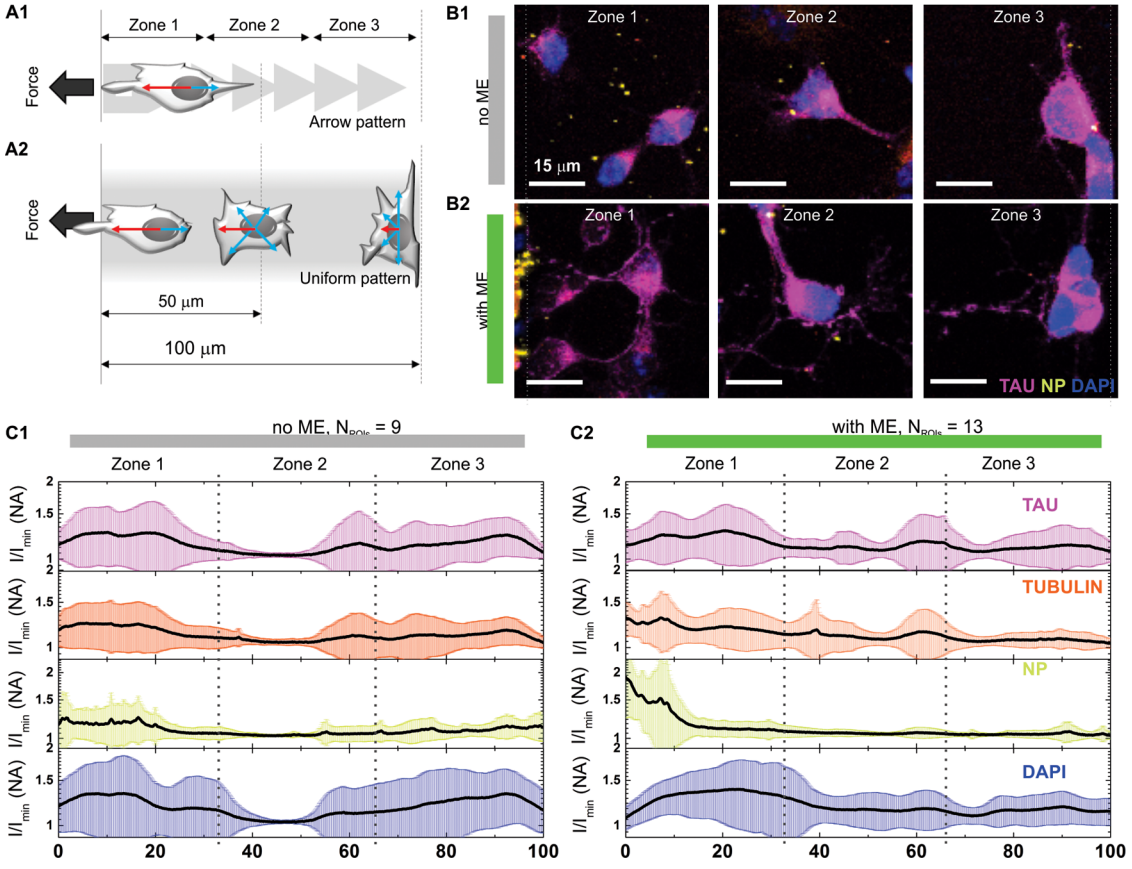

Figure 5. Pattern-constrained cell population study revealed that magnetic gradients impact intracellular localization of tau proteins and can induce cell displacement. (A1, A2) Schematic shows our two different cell-constraining PLL patterns and dimensional parameters for comparing cell effects between our (A1) single-cell ratchet and (A2) cell population stripe pattern. Depending on the distance to the MEs, three different force zones can be introduced across the cell pattern areas. Zone 1: large forces; zone 2: medium forces; zone 3: very low forces. (B1, B2) Pseudocolored laser confocal images show representative neuron cell morphology across the 100 μm wide PLL stripe pattern in different force zones with (B1) and without (B2) magnetic gradients after 24 h exposure to low magnetic fields (100 mT). (C1, C2) Averaged and normalized fluorescent signal intensity plots for TAU, MAP2, DAPI stainings, and fMNPs across a 100 μm $\times$ 20 μm ROI show the mean (black line) and standard deviation (color area) (C1: no magnetic gradient, N_{av} = 9 ROI, N_{cells} = 130; C2: with magnetic gradient, ME: 12 μm $\times$ 16 μm, 90° orientation, N_{av} = 13 ROI, N_{cells} = 77) under medium magnetic field condition.

of ~300 pN, which is more than 2 times higher than the initially observed cell displacement threshold (130 pN) from the single-cell study above (Figure 6 and Figure S11). Figure 6 represents force-dependent cell positioning and tau formation on the striped pattern area. A shift of tau can be seen in averaged and normalized intensity plots (I/I_{min}, 1 = background) between 100 and 200 pN (Figure 6A2 and B). The cell nucleus (shift in DAPI signal), however, earliest starts following the shift of tau signal around 300 pN (Figure 6D) and only if a magnetic gradient force is abundant (Figure 6C). Interestingly, it has been hypothesized that tau might play a role in initiating neural cell migration,[51,52] suggesting the induction of pathway-mediated cell migration rather than a purely physical manipulation of cells.

In our experimental data we observed that somata from the cell population are attracted toward MEs in both medium and strong magnetic fields. A uniform magnetic field itself, however, induced no neuronal cell displacement (Figure 6C1, C2, magnetic gradient *versus* no gradient before and after 24 h field exposure). Across multiple stripes, neurons were uniformly distributed when exposed to the three different magnetic field strengths in the absence of MEs (Figure 6D1). Local magnetic gradients impacted neuronal marker distribution across cell populations with 5 $\pm$ 1 neighbors per cell (Figure 6D2, TAU-5, MAP-2, Tubulin) and induced cell displacement above 300 pN, visible as strong orientation of neural cell nuclei and bodies (Figure 6D2, DAPI) toward the fMNP traps (Figure 6D2, NP). From our data we can conclude that a force of >300 pN is necessary to induce cell displacement, when neurons were cultured with up to five cell neighbors, in contrast to the 130 pN needed for the displacement of single cortical neurons.

To exclude a chemical gradient effect due to potentially chemoattractive acting surface functional groups of the fMNPs, we conducted control studies where nanoparticles were first patterned within the magnetic field gradients followed by neuronal cells cultured on top. The results from this study

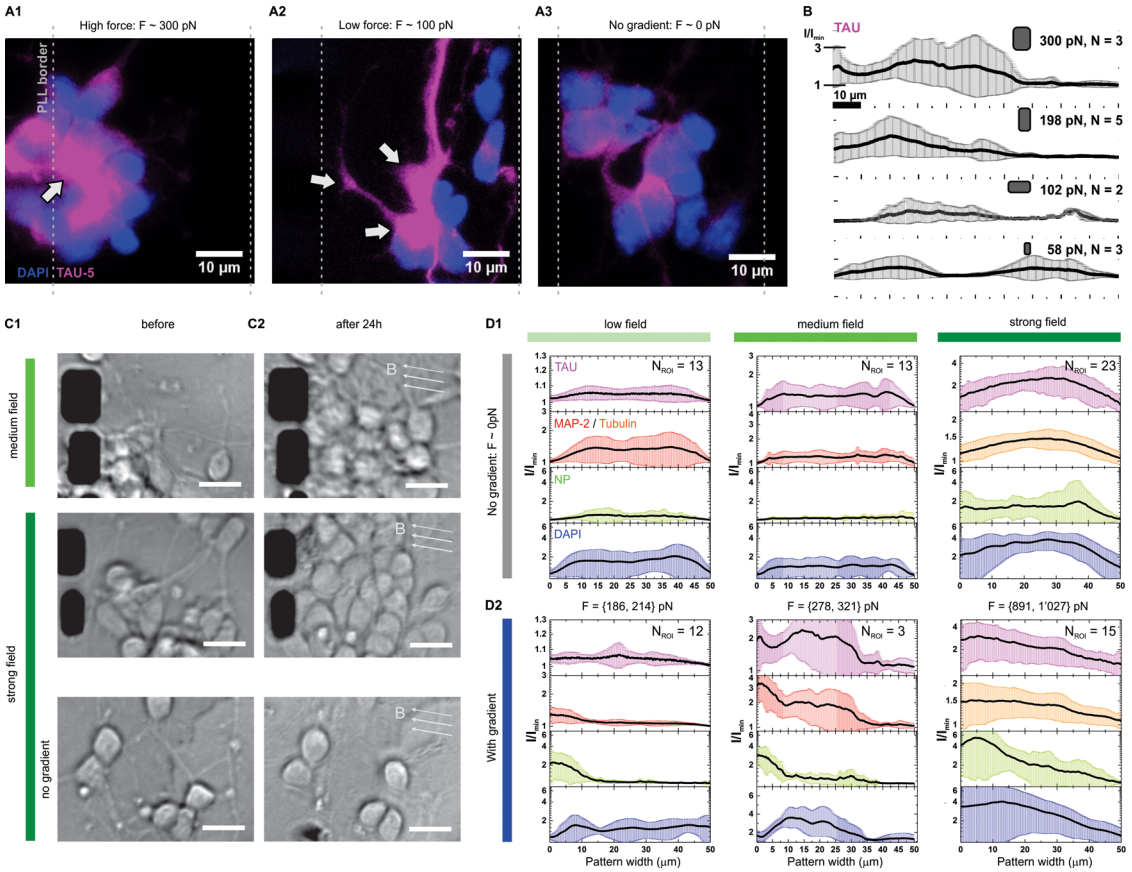

Figure 6. Magnetic field strength affects force-induced cell displacement. (A1−A3) Representative fluorescence images show neuronal cell response on 50 μm wide PLL stripes to different forces scales: (A1) 90° orientation MEs left of the PLL pattern, (A2) 0° orientation MEs left of the PLL pattern, and (A3) no MEs. Arrows highlight increased TAU-5 fluorescence signal. (B) Averaged and normalized TAU-5 fluorescent signal show the mean (black line) and standard deviation (gray area) extracted from 20 μm × 50 μm ROI areas. Higher forces lead to a shift of TAU-5 signal toward the MEs. (C1, C2) Phase contrast images taken right before (C1) applying a permanent external magnetic field and (C2) 24 h after. Medium and strong magnetic field gradients initiate cell accumulation adjacent to the MEs, while strong uniform magnetic fields without MEs did not. Scale bar = 12 μm. (D1, D2) Averaged and normalized fluorescent intensity plots of 50 μm × 20 μm ROIs show the mean (black line) and standard deviation (color area) for TAU-5, MAP-2/Tubulin, fMNP, and DAPI (D1) without magnetic gradients and (D2) next to 12 μm × 16 μm, 90° orientation MEs. Plots demonstrate uniform cell distribution across the PLL pattern (DAPI), uniform fMNP localization (NP), and uniform neural marker distribution (TAU, MAP-2/Tubulin) after 24 h exposure to low (100 mT, N_{av} = 12 ROI), medium (150 mT, N_{av} = 3 ROI, N_{cells} = 40), and strong (480 mT, N_{av} = 15 ROI) fields without gradient forces and induced cell displacement around 300 pN due to increasing fMNP-mediated gradient forces on neurons.

showed no sign of localized tau polarity or specific orientation of neurite outgrowth (see Supporting Information, Figure S12).

In summary, our data confirm that the orientation and strength of cell polarization in the form of a skewed distribution of tau staining occurred with higher magnetic field gradients and decreased with the number of cell neighbors. Furthermore, forces that induced cell displacement occurred above 300 pN within neural cell populations.

CONCLUSION

We have introduced a neuromagnetic chip to study neural cell polarity under fMNP-mediated magnetic forces. Using these chips, we studied single-cell polarity as revealed by the asymmetric distribution of the cytoskeletal protein tau. We identified approximate induced-force thresholds for neuromechanical sensitivity at 4.3 to 70 pN (tau polarity). We also found that forces above 130 pN led to single-cell displacements. In a second set of studies we used cell populations and found that nanoparticle-mediated forces induced cell displacement events at a threshold of 300 pN and above in cell populations with 5 ± 1 neighbors per cell. Our findings suggest that fMNP-mediated magnetic forces can be used to engineer intracellular protein distributions in neurons (specifically to relocate tau protein distributions) and help to define target force ranges for the induction of protein redistribution and cell migration. Broadly, our studies also suggest that nanoparticle-mediated signals can be utilized to encode and supplement neural network development *in vitro* and that magnetic strategies could potentially develop into novel neurotherapeutic approaches, whereby fMNPs guide the restoration of damaged or dysfunctional neurite

networks in inaccessible regions of the central nervous system. Beyond engineering concepts, neuromagnetic chips can yield new insights into mechanotransduction in neural networks.

METHODS

Engineering Magnetic Field Gradients and Characterizing Resultant Magnetic Forces. To scale force magnitudes to a compatible level, several experimental parameters were considered. On the basis of an average cortical neuron cell diameter of 16 μm, magnetic field gradients on the order of 10 000 T/m,[53] and soft mechanical properties of neurons,[54] four different magnetic element geometries were chosen: (i) 12 μm × 16 μm, (ii) 8 μm × 16 μm, (iii) 4 μm × 16 μm, and (iv) 4 μm × 8 μm, with three varied orientations in relation to the magnetic field (magnetic flux density, Figure 2D1). In our figures the different orientations of MEs were encoded with (i) 0°, *L* = length; (ii) 45°, *R* = rotational; and (iii) 90°, *V* = vertical.

A superparamagnetic particle within a magnetic flux density gradient, referred to as magnetic gradient in the main text (∇B), experiences a magnetic forces (*F*, eq 1) due to its magnetic momentum (*m*).

$$F = \nabla(m \cdot B) \tag{1}$$

Superparamagnetic micro- and nanoparticles in high-gradient magnetic fields often form clusters, where the exerted force sums up based on the number *i* of agglomerated particles with a particle volume V_p. From eq 2, we derived our resulting force (*F*) where $M_{p,sat}$ is the particle magnetization under magnetic saturation, $\nabla H(x, y, z)$ the gradient of the magnetic field strength, and μ_0 the vacuum permeability.[55]

$$F = \mu_0 \sum_{i=1}^{n} V_{p,i} M_{p,i,sat} \nabla H(x, y, z) \tag{2}$$

The different force strengths of our multisized and oriented MEs were characterized using fluorescently labeled 1 μm diameter superparamagnetic iron oxide beads (MP, Chemicell, screenMAG, 45.5% Fe content, lot: 0502/13). According to the manufacturer, the bead saturation magnetization (M_s) was determined to be 3.8 mT ($M_{s,bead}$). We extracted magnetic forces based on a balancing force act of the magnetic and Stokes forces at the bead, which is moving in a biological medium (PBS, $\eta = 1 \times 10^{-3}$ Pa s) within a magnetic gradient.[56] Since the externally applied permanent magnet generates a magnetic field at the MEs greater than the magnetization of the beads, we assumed a linear relationship (eq 2) between magnetic force (*F*), permeability (μ_0), and the magnetic field gradient ($\nabla H(x,y,z)$, in Supporting Information Figure S2).

Magnetic bead movement was monitored using fluorescent and phase contrast microscopy with the magnet slightly shifted to open the optical pathway. We extracted bead velocities ($v_=$) parallel to the PSR-5 surface on our neuromagnetic chip with a treated PSR-5 surface of 2% Pluronic F127. Using MTrack[57] for ImageJ bead trajectories were measured from time series (11 fps) and velocities extracted. We assumed frictional movement as described by Schaeffer *et al*. using a Faxen's law coefficient $\lambda_{Faxen} = 2.29$ (eq 3)[58] to calculate forces along trajectory positions (in Supporting Information Figure S3).

$$F = 6\lambda_{Faxen}\pi\mu_0 r_{h,p} v_= \tag{3}$$

On the basis of a possible exponential decay of the gradient field and the linear relation between field and force (eq 2), estimated forces were assumed to scale down exponentially with distance from the MEs (Figure 2D2, eq 4).

$$\ln F(x) = f + Rx \tag{4}$$

Nanoparticle (NP)-induced forces (F_{NP}) were estimated based on magnetic nanoparticle momentum (m_{NP}) in relation to magnetic bead momentum (m_{MP}, eq 1) considering magnetic dipole theory; see eq 5, where *r* is the radius of the particles, core% the iron core percentage, and ρ the material density (data from manufacturer, see the Supporting Information).

$$F_{NP} = F_{MP}\frac{m_{NP}}{m_{MP}} \text{ with } \frac{m_{NP}}{m_{MP}} = \frac{M_{sat,NP}\rho_{NP}\text{core}\%_{NP}r_{NP}^3}{M_{sat,MP}\rho_{MP}\text{core}\%_{MP}r_{MP}^3} \tag{5}$$

Fabrication of the Neuromagnetic Chip. Chip fabrication was based on the micromagnetic slides published by Tseng *et al*.[33] with modifications in the photoresist composition and patterning technique (Supporting Information Figure S1). For poly-L-lysine patterning, a 1 μm AZ5214 layer was spun on the PSR-5 resist, underbaked (40−50 s, 95 °C), photolithographically patterned, and developed (AZ400 K/water solution, 1:4). The opened PSR surface was O_2 plasma activated (38 W, 30 s, 500 mTorr), and AZ5214 was removed through a 100% acetone rinse. We used competitive coadsorption[59] of Pluronic F127 and PLL to hydrophobic and hydrophilic photoresist surfaces. Single-cell patterning was inspired by micropatterned ratchets.[20,44] Our ratchet design consisted of one square (15 μm × 15 μm, P0) and arrow-shaped ratchets (14.5 μm × 15 μm, P1) with one (P2) to five (P6) repetitions of triangles for directional neurite outgrowth (Supporting Information Figure S9). Cell population patterning was established on stripes of 20, 50, 100, 150, and 200 μm; 300 μm widths, 2 mm length, of which 20, 50, and 100 μm were relevant for our experimental evaluation.

Dissociated Neuronal Cell Culture. For our cortical neuron culture, cortical hemispheres were dissected from whole rat brains (E18, BrainBits) and dissociated with 10% (v/v) papain (*Carica papaya*, Roche) in Hibernate-E (BrainBits). We seeded our cells at a final concentration of 500 000 cells/mL (0.5 mL seeded in chip) on the neuromagnetic chip and incubated them overnight. At 1 DIV, cortical cells were exposed to a mixture of three types of functionalized fluoresecent superparamagnetic nanoparticles (fMNP, Chemicell, 1:1:1 in Neurobasal, 1% PenStrep, 1% GlutaMAX, 2% B-27, 10 μg/mL each), (1) glucuronic acid, (2) starch, and (3) chitosan, and incubated for up to 6 h. After washing, the cultures were exposed to three strengths of magnetic fields for up to 24 h: 100 mT (1/2 in. × 1/2 in. × 1/8 in., Apex Magnets), 150 mT (1/2 in. × 1/2 in. × 1/2 in., Apex Magnets), and 480 mT (1 in. × 1 in. × 1 in., K&J Magnetics) rare earth magnets.

Selecting fMNPs for Cortical Neuron Interrogation. FMNPs were selected based on nanoparticle uptake studies with glucuronic acid-functionalized nanoparticles found in the literature[37] or previously reported functional groups such as chitosan[39] and starch[60] with nondegenerative effects on neurons. In control experiments, fMNP uptake of fluorescent glucuronic acid-, starch-, and chitosan-coated superparamagnetic dextran particles (Chemicell) was monitored over 24 h, and a final mixture of all functional groups with a 1:1:1 ratio was used in our experimental study. FMNP location and astrogliosis (GFAP positive cell immunostaining) was monitored for each single fMNP type and the mixture of all three types of fMNPs at a final concentration of 30 μg/mL (Supporting Information Figure S5, Table S2). Glucuronic acid-coated nanoparticles appeared sparsely in only a few neurons, which confirmed observations reported by Pinkernell *et al*.[37] and Steketee *et al*.[36] Starch-coated fMNPs were mainly visible at the tip of neurites, while chitosan-coated fMNPs were visible along neurites and in the soma and were especially visible between cell−cell contact points (Supporting Information Figure S5).

Immunofluorescent Labeling. Cortical neurons were washed with Dulbecco's phosphate-buffered saline (DPBS with magnesium and calcium, Gibco) and fixed for 20 min with paraformaldehyde (4% (v/v) PFA/PBS, Santa Cruz Biotechnologies), permeabilized with 0.1% Triton-X/DPBS and 3% BSA for 10 min, and blocked with 3% goat serum in 1% BSA/DPBS. Primary antibodies were incubated overnight (4 °C) in 3% goat serum and 0.5% Tween-20 in 1% BSA/DPBS, and secondary antibodies for 2 h (room temperature). Primary antibodies utilized

included rabbit anti-GFAP (1:200), chicken anti-MAP2 (1:200), mouse anti-TAU-5 (1:200), and Fluor488 anti-Tubulin-beta-III, and secondary antibodies utilized included DyLight 405 anti-rabbit IgG (1:500), CY-5 anti-mouse (1:300), and Alexa Fluo568 anti-chicken (1:500).

Image Analysis and Statistical Evaluation. Tau protein distribution in single neurons was quantified by measuring an orientation vector from the center of the nucleus to the centroid of neuronal tau staining in ImageJ based on 12-bit fluorescent and phase contrast images. fMNPs (FITC channel) that were taken up were quantified through particle counting, when co-localized with tau staining. Single-neuron location was rated on proximity to ME (6 = farthest, 1 = closest) and geometry of the pattern (P1−P6); fMNPs taken up were categorized by the following particle cluster ($A_{cluster}$) code (bin 0: no fMNP, bin I: few nanoparticles, $A_{cluster} < 0.5\ \mu m^2$, bin II: few clusters, $A_{cluster} = 0.5-1.0\ \mu m^2$, bin III: multiple dots, $A_{cluster} = 1.0-2.0\ \mu m^2$, bin IV: all clusters, $A_{cluster} > 2.0\ \mu m^2$). Cell population behavior was analyzed based on normalized fluorescent signal distribution of fluorescent stainings (I/I_{min}) across the PLL pattern width from individual channels. From the orientation vector, absolute vector length, *x*-projected vector length, and orientation angle were extracted. Histogram plots for *x*-projected vector length show a length distribution in 13 length bins between −6 and 6 μm. Histogram plots for orientation angle show angle distribution in four angle bins of 90° around 45°, 135°, 225°, and 315°. Histogram plots were tested for normality using D'Agostino's K-squared test based on skewness, kurtosis, and omnibus. As the location of protein distribution is restricted by the cell membrane and most neuronal proteins can be found somewhere in the soma, we expected a shift in median position rather than a significance in mean location or variance. Significance of tau protein orientation was tested using the nonparametric one-sample Wilcoxon singed rank test with null-hypothesis median ≥ 0 and hypothesis median < 0, $p < 0.05$ (OriginPro 9). Significance of tau protein polarization (how far from the nucleus center point is the maximum signal of tau protein located) was tested on absolute vector length after a normality test using either one-way ANOVA, $p < 0.05$ (no rejection of normality), or nonparametric Kruskal−Wallis ANOVA, $p < 0.05$ (normality rejected). Normalized signal intensity plots I/I_{min} were normality tested, and signal distributions compared with the Kolmogorov−Smirnov test ($F(x) \neq G(x)$, $p < 0.001$) and Friedman ANOVA ($p < 0.005$).

Conflict of Interest: The authors declare no competing financial interest.

Acknowledgment. The authors wish to thank NSF Nanolab core facility for cleanroom assistance, J. Harrison for electroplating maintenance, and K. Chan for research assistance with initial nanoparticle experiments. Confocal laser scanning microscopy was performed at the CNSI Advanced Light Microscopy/Spectroscopy Shared Resource Facility at UCLA, supported with funding from NIH-NCRR shared resources grant (CJX1-443835-WS-29646) and NSF Major Research Instrumentation grant (CHE-0722519). A.K. thanks the Swiss National Science Foundation (SNSF) for supporting this project under the grant P300P2_147753. Further, this work was partially supported through the NIH Director's New Innovator Grant (1DP2OD007113). A.K., P.T., A.C., F.S., and D.D.C. were involved in conceptual and experimental discussion. A.K. designed the neuromagnetic chips, the MEs, and experiments. A.K., P.T., and C.M. fabricated chips. A.C. tested different coatings. A.K. performed neural cultures and experiments. A.K. and C.G. characterized ME forces, performed image acquisitions, and analyzed experimental data. A.K. drafted and revised the manuscript with all coauthors.

Supporting Information Available: Additional material about chip design, force methodology, nanoparticle uptake in primary cortical neurons, single-cell evaluation, statistical data distribution, and control experiments for force sensitivity within cell population are provided. This material is available free of charge *via* the Internet at http://pubs.acs.org.

REFERENCES AND NOTES

1. Shelly, M.; Cancedda, L.; Lim, Byung K.; Popescu, A. T.; Cheng, P.-l.; Gao, H.; Poo, M.-m. Semaphorin3A Regulates Neuronal Polarization by Suppressing Axon Formation and Promoting Dendrite Growth. *Neuron* **2011**, *71*, 433–446.
2. Halder, G.; Dupont, S.; Piccolo, S. Transduction of Mechanical and Cytoskeletal Cues by YAP and TAZ. *Nat. Rev. Mol. Cell Biol.* **2012**, *13*, 591–600.
3. Mammoto, T.; Ingber, D. E. Mechanical Control of Tissue and Organ Development. *Development* **2010**, *137*, 1407–1420.
4. Hilgetag, C. C.; Barbas, H. Developmental Mechanics of the Primate Cerebral Cortex. *Anat. Embryol.* **2005**, *210*, 411–417.
5. Howard, J.; Grill, S. W.; Bois, J. S. Turing's Next Steps: The Mechanochemical Basis of Morphogenesis. *Nat. Rev. Mol. Cell Biol.* **2011**, *12*, 392–398.
6. Franze, K.; Janmey, P. A.; Guck, J. Mechanics in Neuronal Development and Repair. *Annu. Rev. Biomed. Eng.* **2013**, *15*, 227–251.
7. Stiess, M.; Bradke, F. Neuronal Polarization: The Cytoskeleton Leads the Way. *Dev. Neurobiol.* **2011**, *71*, 430–444.
8. Bradke, F.; Dotti, C. G. Neuronal Polarity: Vectorial Cytoplasmic Flow Precedes Axon Formation. *Neuron* **1997**, *19*, 1175–1186.
9. Vaccarino, F. M.; Smith, K. M. Increased Brain Size in Autism - What It Will Take to Solve a Mystery. *Biol. Psychiatry* **2009**, *66*, 313–315.
10. Bullmore, E.; Sporns, O. Complex Brain Networks: Graph Theoretical Analysis of Structural and Functional Systems. *Nat. Rev. Neurosci.* **2009**, *10*, 186–198.
11. Alivisatos, A. P.; Andrews, A. M.; Boyden, E. S.; Chun, M.; Church, G. M.; Deisseroth, K.; Donoghue, J. P.; Fraser, S. E.; Lippincott-Schwartz, J.; Looger, L. L.; *et al.* Nanotools for Neuroscience and Brain Activity Mapping. *ACS Nano* **2013**, *7*, 1850–1866.
12. Roy, J.; Kennedy, T. E.; Costantino, S. Engineered Cell Culture Substrates for Axon Guidance Studies: Moving Beyond Proof of Concept. *Lab Chip* **2013**, *13*, 498–508.
13. Millet, L. J.; Gillette, M. U. New Perspectives on Neuronal Development *via* Microfluidic Environments. *Trends Neurosci.* **2013**, *35*, 752–761.
14. Sun, Y.; Huang, Z.; Liu, W.; Yang, K.; Sun, K.; Xing, S.; Wang, D.; Zhang, W.; Jiang, X. Surface Coating as a Key Parameter in Engineering Neuronal Network Structures *in Vitro*. *Biointerphases* **2012**, *7*, 1–14.
15. Millet, L. J.; Stewart, M. E.; Nuzzo, R. G.; Gillette, M. U. Guiding Neuron Development with Planar Surface Gradients of Substrate Cues Deposited Using Microfluidic Devices. *Lab Chip* **2010**, *10*, 1525–1535.
16. Bhattacharjee, N.; Li, N.; Keenan, T. M.; Folch, A. A Neuron-Benign Microfluidic Gradient Generator for Studying the Response of Mammalian Neurons towards Axon Guidance Factors. *Integr. Biol.* **2011**, *2*, 669–679.
17. Esch, T.; Lemmon, V.; Banker, G. Local Presentation of Substrate Molecules Directs Axon Specification by Cultured Hippocampal Neurons. *J. Neurosci.* **1999**, *19*, 6417–6426.
18. Jee, J. M.; Yoonkey, N. Geometric Effect of Cell Adhesive Polygonal Micropatterns on Neuritogenesis and Axon Guidance. *J. Neural Eng.* **2012**, *9*, 1–10.
19. Fricke, R.; Zentis, P. D.; Rajappa, L. T.; Hofmann, B.; Banzet, M.; Offenhaeusser, A.; Meffert, S. H. Axon Guidance of Rat Cortical Neurons by Microcontact Printed Gradients. *Biomaterials* **2012**, *32*, 2070–2076.
20. Scott, M. A.; Wissner-Gross, Z. D.; Yanik, M. F. Ultra-Rapid Laser Protein Micropatterning: Screening for Directed Polarization of Single Neurons. *Lab Chip* **2012**, *12*, 2265–2276.
21. Hilgetag, C. C.; Barbas, H. Role of Mechanical Factors in the Morphology of the Primate Cerebral Cortex. *PLoS Comput. Biol.* **2006**, *2*, 146–159.
22. Bok, S. T. Curvature of the cerebral cortex. In *Histonomy of the Cerebral Cortex*; Elsevier Pub. Co.: Amsterdam, 1959; pp 1−434.
23. Tyler, W. J. The Mechanobiology of Brain Function. *Nat. Rev. Neurosci.* **2012**, *13*, 867–878.
24. Fuhs, T.; Reuter, L.; Vonderhaid, I.; Claudepierre, T.; Käs, J. A. Inherently Slow and Weak forward Forces of Neuronal

Growth Cones Measured by a Drift-Stabilized Atomic Force Microscope. *Cytoskeleton* **2013**, *70*, 44–53.
25. Fass, J. N.; Odde, D. J. Tensile Force-Dependent Neurite Elicitation *via* Anti-Beta1 Integrin Antibody-Coated Magnetic Beads. *Biophys. J.* **2003**, *85*, 623–636.
26. Pfister, B. J.; Iwata, A.; Meaney, D. F.; Smith, D. H. Extreme Stretch Growth of Integrated Axons. *J. Neurosci.* **2004**, *24*, 7978–7983.
27. Lamoureux, P.; Heidemann, S.; Miller, K. E. Mechanical Manipulation of Neurons to Control Axonal Development. *J. Vis. Exp.* **2011**, e2509.
28. Bernick, K. B.; Prevost, T. P.; Suresh, S.; Socrate, S. Biomechanics of Single Cortical Neurons. *Acta Biomater.* **2011**, *7*, 1210–1219.
29. Nguyen, T. D.; Hogue, I. B.; Cung, K.; Purohit, P. K.; McAlpine, M. C. Tension-Induced Neurite Growth in Microfluidic Channels. *Lab Chip* **2013**, *13*, 3735–3740.
30. Lamoureux, P.; Ruthel, G.; Buxbaum, R. E.; Heidemann, S. R. Mechanical Tension Can Specify Axonal Fate in Hippocampal Neurons. *J. Cell Biol.* **2002**, *159*, 499–508.
31. Bray, D. Axonal Growth in Response to Experimentally Applied Mechanical Tension. *Dev. Biol.* **1984**, *102*, 379–389.
32. de Vries, A. H. B.; Krenn, B. E.; van Driel, R.; Kanger, J. S. Micro Magnetic Tweezers for Nanomanipulation inside Live Cells. *Biophys. J.* **2005**, *88*, 2137–2144.
33. Tseng, P.; Judy, J. W.; Di Carlo, D. Magnetic Nanoparticle-Mediated Massively Parallel Mechanical Modulation of Single-Cell Behavior. *Nat. Methods* **2012**, *9*, 1113–1119.
34. Wang, E. C.; Wang, A. Z. Nanoparticles and Their Applications in Cell and Molecular Biology. *Integr. Biol.* **2014**, *6*, 9–26.
35. Etoc, F.; Lisse, D.; Bellaiche, Y.; Piehler, J.; Coppey, M.; Dahan, M. Subcellular Control of Rac-GTPase Signalling by Magnetogenetic Manipulation inside Living Cells. *Nat. Nanotechnol.* **2013**, *8*, 193–198.
36. Steketee, M. B.; Moysidis, S. N.; Jin, X.-L.; Weinstein, J. E.; Pita-Thomas, W.; Raju, H. B.; Iqbal, S.; Goldberg, J. L. Nanoparticle-Mediated Signaling Endosome Localization Regulates Growth Cone Motility and Neurite Growth. *Proc. Natl. Acad. Sci. U.S.A.* **2011**, *108*, 19042–19047.
37. Pinkernelle, J.; Calatayud, P.; Goya, G.; Fansa, H.; Keilhoff, G. Magnetic Nanoparticles in Primary Neural Cell Cultures Are Mainly Taken up by Microglia. *BMC Neurosci.* **2012**, *13*, 32–42.
38. Riggio, C.; Calatayud, M. P.; Hoskins, C.; Pinkernelle, J.; Sanz, B.; Torres, T. E.; Ibarra, M. R.; Wang, L.; Keilhoff, G.; Goya, G. F.; *et al.* Poly-L-Lysine-Coated Magnetic Nanoparticles as Intracellular Actuators for Neural Guidance. *Int. J. Nanomed.* **2012**, *7*, 3155–3166.
39. Yue, Z.-G.; Wei, W.; Lv, P.-P.; Yue, H.; Wang, L.-Y.; Su, Z.-G.; Ma, G.-H. Surface Charge Affects Cellular Uptake and Intracellular Trafficking of Chitosan-Based Nanoparticles. *Biomacromolecules* **2011**, *12*, 2440–2446.
40. Riggio, C.; Calatayud, M. P.; Giannaccini, M.; Sanz, B.; Torres, T. E.; Fernández-Pacheco, R.; Ripoli, A.; Ibarra, M. R.; Dente, L.; Cuschieri, A.; *et al.* The Orientation of the Neuronal Growth Process Can Be Directed *via* Magnetic Nanoparticles under an Applied Magnetic Field. *Nanomedicine: NBM* **2014**, *10*, 1549–1558.
41. Pai, J.-H.; Wang, Y.; Salazar, G. T. A.; Sims, C. E.; Bachman, M.; Li, G. P.; Allbritton, N. L. Photoresist with Low Fluorescence for Bioanalytical Applications. *Anal. Chem.* **2007**, *79*, 8774–8780.
42. Cheng, Q.; Komvopoulos, K.; Li, S. Surface Chemical Patterning for Long-Term Single-Cell Culture. *J. Biomed. Mater. Res., Part A* **2010**, *96A*, 507–512.
43. Detrait, E.; Lhoest, J. B.; Bertrand, P.; van den Bosch de Aguilar, P. Fibronectin-Pluronic Coadsorption on a Polystyrene Surface with Increasing Hydrophobicity: Relationship to Cell Adhesion. *J. Biomed. Mater. Res.* **1999**, *45*, 404–413.
44. Mahmud, G.; Campbell, C. J.; Bishop, K. J. M.; Komarova, Y. A.; Chaga, O.; Soh, S.; Huda, S.; Kandere-Grzybowska, K.; Grzybowski, B. A. Directing Cell Motions on Micropatterned Ratchets. *Nat. Phys.* **2009**, *5*, 606–612.
45. Arimura, N.; Kaibuchi, K. Neuronal Polarity: From Extracellular Signals to Intracellular Mechanisms. *Nat. Rev. Neurosci.* **2007**, *8*, 194–205.
46. Roth, S.; Bisbal, M.; Brocard, J.; Bugnicourt, G.; Saoudi, Y.; Andrieux, A.; Gory-Fauré, S.; Villard, C. How Morphological Constraints Affect Axonal Polarity in Mouse Neurons. *PLoS One* **2012**, *7*, e33623.
47. Konzack, S.; Thies, E.; Marx, A.; Mandelkow, E.-M.; Mandelkow, E. Swimming against the Tide: Mobility of the Microtubule-Associated Protein Tau in Neurons. *J. Neurosci.* **2007**, *27*, 9916–9927.
48. Frandemiche, M. L.; De Seranno, S.; Rush, T.; Borel, E.; Elie, A.; Arnal, I.; Lanté, F.; Buisson, A. Activity-Dependent Tau Protein Translocation to Excitatory Synapse Is Disrupted by Exposure to Amyloid-Beta Oligomers. *J. Neurosci.* **2014**, *34*, 6084–6097.
49. Gomez, N.; Chen, S.; Schmidt, C. E. Polarization of Hippocampal Neurons with Competitive Surface Stimuli: Contact Guidance Cues Are Preferred over Chemical Ligands. *J. R. Soc., Interface* **2007**, *4*, 223–233.
50. Shelly, M.; Lim, B. K.; Cancedda, L.; Heilshorn, S. C.; Gao, H.; Poo, M.-m. Local and Long-Range Reciprocal Regulation of cAMP and cGMP in Axon/Dendrite Formation. *Science* **2010**, *327*, 547–552.
51. Sapir, T.; Frotscher, M.; Levy, T.; Mandelkow, E.-M.; Reiner, O. Tau's Role in the Developing Brain: Implications for Intellectual Disability. *Hum. Mol. Genet.* **2012**, *21*, 1681–1692.
52. Sakakibara, A.; Ando, R.; Sapir, T.; Tanaka, T. Microtubule Dynamics in Neuronal Morphogenesis. *Open Biol.* **2013**, *3*, 1–9.
53. Hatch, G. P.; Stelter, R. E. Magnetic Design Considerations for Devices and Particles Used for Biological High-Gradient Magnetic Separation (HGMS) Systems. *J. Magn. Magn. Mater.* **2001**, *225*, 262–276.
54. Spedden, E.; White, J. D.; Naumova, E. N.; Kaplan, D. L.; Staii, C. Elasticity Maps of Living Neurons Measured by Combined Fluorescence and Atomic Force Microscopy. *Biophys. J.* **2012**, *103*, 868–877.
55. Blaire, G.; Masse, A.; Zanini, L.; Gaude, V.; Delshadi, S.; Honegger, T.; Peyrade, D.; Weidenhaupt, M.; Dumas-Bouchiat, F.; Bruckert, F.; *et al.* Hybrid Bio-Mag-MEMs Combining Magnetophoresis and Dielectrophoresis. *Eur. Phys. J. B* **2013**, *86*, 1–6.
56. Shevkoplyas, S. S.; Siegel, A. C.; Westervelt, R. M.; Prentiss, M. G.; Whitesides, G. M. The Force Acting on a Superparamagnetic Bead Due to an Applied Magnetic Field. *Lab Chip* **2007**, *7*, 1294–1302.
57. Meijering, E.; Dzyubachyk, O.; Smal, I. Methods for Cell and Particle Tracking. In *Methods in Enzymology*; Academic Press: New York, 2012; Vol. 504, pp 183−200.
58. Schaeffer, E.; Norrelykke, S. F.; Howard, J. Surface Forces and Drag Coefficients of Microspheres near a Plane Surface Measured with Optical Tweezers. *Langmuir* **2007**, *23*, 3654–3665.
59. Cheng, Q.; Komvopoulos, K.; Li, S. Surface Chemical Patterning for Long-Term Single-Cell Culture. *J. Biomed. Mater. Res., Part A* **2011**, *96A*, 507–512.
60. Nakai, J.; Kawasaki, Y. Studies on the Mechanism Determining the Course of Nerve Fibers in Tissue Culture. *Z. Zellforsch. Mikrosk. Anat.* **1959**, *51*, 108–122.